New Phytologist

Research

Methods

Intercomparison of methods for estimating leaf inclination angle distribution with terrestrial lidar for broadleaf tree species

Chris Mutugi Murithi[1,2]*, Jan Pisek[1]*, Daniel Schraik[3], Brian N. Bailey[4], Jing Liu[5,6], Atticus E. L. Stovall[7,8], Matheus Boni Vicari[9], Guang Zheng[10] and Andrew Skidmore[2,11]

[1]Tartu Observatory, University of Tartu, 61602, Tõravere, Estonia; [2]Faculty of Geo-Information Science and Earth Observation (ITC), University of Twente, P.O. Box 217, 7500 AE, Enschede, the Netherlands; [3]Natural Resources Institute Finland, Latokartanonkaari 9, 00790, Helsinki, Finland; [4]Department of Plant Sciences, University of California, Davis, Davis, CA 95616, USA; [5]Key Laboratory of Virtual Geographic Environment, (Nanjing Normal University), Ministry of Education, Nanjing, 210023, China; [6]Jiangsu Center for Collaborative Innovation in Geographical Information Resource Development and Application, Nanjing, 210023, China; [7]Earth System Science Interdisciplinary Center, University of Maryland, College Park, MD 20706, USA; [8]Biospheric Sciences, NASA Goddard Space Flight Center, Greenbelt, MD 20771, USA; [9]Mantis-AI, São Paulo, SP, 04003-000, Brazil; [10]International Institute for Earth System Science, Nanjing University, 210023, Nanjing, China; [11]School of Natural Sciences, Macquarie University, 12 Wally's Walk, Sydney, NSW, 2109, Australia

Author for correspondence:
Jan Pisek
Email: janpisek@gmail.com

Received: *12 March 2025*
Accepted: *22 June 2025*

New Phytologist (2025) **248:** 415–430
doi: 10.1111/nph.70379

Key words: 3D, leaf inclination angle distribution (LIAD), leveled digital photography (LDP), light detection and ranging (LiDAR), terrestrial laser scanning (TLS).

Summary

- Leaf inclination angle distribution (LIAD) is a fundamental parameter of models that illustrate the energy and mass exchanges for vegetation at all scales. Terrestrial laser scanning (TLS) instruments have emerged as valuable tools for acquiring detailed measurements of canopy structure. Here, we present the first intercomparison of the available LIAD estimation techniques using TLS data.
- The available LIAD estimation techniques were evaluated using TLS point clouds of both real and synthetic trees covering the full range of the existing LIAD types. The performance of the proposed TLS-based methods was also compared with the established, non-TLS-based leveled digital photography approach.
- The study highlighted that the algorithms that used merged point clouds performed better than their single-scan counterparts. TLS offered a more comprehensive representation of the canopy structure and overcame the limitations of the traditional leveled digital photography approach for both real and simulated trees.
- This study may serve as a template for establishing benchmark datasets, evaluation protocols, and accessibility of algorithms that could facilitate systematic comparisons of LIAD estimation algorithms. This collaborative effort promotes fairness, reproducibility, and the advancement of LIAD estimation techniques by enabling researchers to identify strengths, weaknesses, and areas for improvement in their algorithms.

Introduction

Leaf inclination angle (i.e. inclination of the leaf to the horizontal plane, or the angle between the leaf surface normal and zenith) distribution (LIAD) is a fundamental parameter of models that illustrate the energy and mass exchanges for vegetation at all scales (Li *et al.*, 2018a; Vicari *et al.*, 2019). LIAD is considered integral to the spectral reflectance and radiation transmission properties of vegetation canopies. LIAD affects radiation interception, evapotranspiration, and photosynthesis (Ross, 1981; Myneni *et al.*, 1989; Asner, 1998; Utsugi *et al.*, 2006; Stuckens *et al.*, 2009; Niinemets, 2010; Yang *et al.*, 2023). Plants adjust leaf angle to acquire resources such as light or adapt to environmental changes (Darwin, 1881; Ehleringer & Forseth, 1980; Muraoka *et al.*, 1998). Moreover, the leaf inclination angle can indicate plant stress, such as water deficiency, severe heat, or a disease (Omasa *et al.*, 2007; Konishi *et al.*, 2009). Despite its importance, challenges in measuring LIAD have caused it to be one of the most poorly characterized parameters in land surface models (Ollinger, 2011). It is typically presumed to follow specific probability distributions (such as isotropic/spherical), or alternatively is simplified using predefined mathematical functions without considering its spatial (e.g. vertical) or temporal variation (Liu *et al.*, 2019; Vicari *et al.*, 2019).

*These authors share joint first authorship.

Terrestrial laser scanning (TLS) instruments have been increasingly used when acquiring measurements of the canopy structure (Hosoi & Omasa, 2006; Yang *et al.*, 2013). TLS instruments are ground-based devices that use light detection and ranging (LiDAR) to either measure the distance to a target based on the time recorded between the emission of laser pulses and their return (Disney, 2019; Koma *et al.*, 2021; Kissling *et al.*, 2022) or the phase difference between the sent and received waveforms (Grotti *et al.*, 2020). These instruments also support field data collection to gather species trait information for individual plants and allow us to move beyond stand-level metrics (Kellner *et al.*, 2019). Observations on individual plant traits, such as mean leaf angle, crown density, and rugosity (McNeil *et al.*, 2023), can be integrated with biological knowledge to enhance our understanding of fundamental plant biology and Earth-system science. Various methods have been proposed for retrieving leaf inclination angle distribution information from LiDAR data (e.g. Hosoi & Omasa, 2006; Zheng & Moskal, 2012; Zhao *et al.*, 2015; Jin *et al.*, 2016; Bailey & Mahaffee, 2017; Li *et al.*, 2018b; Itakura & Hosoi, 2019; Liu *et al.*, 2019; Vicari *et al.*, 2019; Stovall *et al.*, 2021), yet no intercomparison has been reported so far.

TLS-based approaches to LIAD estimation may provide several advantages compared to the established, non-TLS-based leveled digital photography (LDP) approach (Ryu *et al.*, 2010; Pisek *et al.*, 2011). The LDP method was previously shown to be limited by its manual, nonautomated selection of appropriate leaves for LIAD estimation, as previously noted by Vicari *et al.* (2019). Another drawback of the LDP method is its limited accuracy in estimating LIAD for curved leaves, as it typically involves the assignment of a single angle to leaves that can have a wide range of surface inclinations within a single leaf. TLS methods offer a more objective, transparent, accurate, comprehensive, and reproducible approach to measuring a critical 'crown-scale' functional trait in individual trees. This study aims to test, compare, and validate available TLS-based LIAD estimation methods using terrestrial LiDAR data. The two specific objectives are to: (1) compare the available LIAD estimation techniques using TLS point clouds of both real and synthetic trees covering the full range of the existing LIAD types; and (2) evaluate the performance of the TLS-based methods with the established, non-TLS-based LDP approach (Ryu *et al.*, 2010; Pisek *et al.*, 2011).

The three specific research questions are:

(**1**) Is there an agreement between the various methods in retrieving LIAD information from LiDAR data?

(**2**) What are the strengths and limitations of the individual methods used to extract LIAD information from LiDAR data?

(**3**) What might be the recommendations for improving LIAD retrieval with LiDAR data in the future?

Materials and Methods

LIAD estimation algorithms

This intercomparison includes TLS-based LIAD estimation techniques introduced and codes made available by Zheng & Moskal (2012), Bailey & Mahaffee (2017), Liu *et al.* (2019), Vicari *et al.* (2019), Stovall *et al.* (2021), and the Point Cloud Library (PCL normals estimation) (Point Cloud Library, n.d.). Each of the included methods is briefly described below.

Zheng & Moskal (2012) applied a total least squares fitting technique to reconstruct leaf normal vectors by fitting a plane to its six neighboring LiDAR leaf intersection points. Zheng & Moskal (2012) reported good performance of their algorithm in estimating the angular variability of a small plant or seedling, with a 78.51% accuracy. However, in the same study, a prediction accuracy of 57.28% indicated less agreement for a mature tree in its natural environment. The algorithm is based on the Computational Geometry Algorithms Library (CGAL). This open-source C++ library grants easy access to efficient and reliable geometric algorithms, such as the estimation of normals (The Computational Geometry Algorithms Library, n.d.).

Bailey & Mahaffee (2017) developed a LIAD estimation method based on the triangulation of LiDAR leaf intersection points that directly calculates the normal vector of the plane formed by three adjacent points. Potential advantages of this approach relative to plane fitting methods are that a triangle represents the fewest points needed to obtain a leaf angle estimation, and thus is likely to yield more angle estimates in areas of low point density. It also allows for area-based weighting of the leaf angle estimates, which corrects for the bias toward leaves with normals closer to the beam scanning direction (Bailey & Mahaffee, 2017). The algorithm is based on the Helios simulation system, a flexible modeling framework that utilizes a C++ API to handle tasks like managing geometry and associated data structures and estimating leaf area density based on the measured LIAD (Bailey, 2019; Helios Documentation v.1.2.58, n.d.).

Liu *et al.* (2019) considered the leaf size in the estimation of LIAD. They initially classified point clouds based on geometric and radiometric attributes, separating leaves from woody material to facilitate the retrieval of LIAD without the effects of the nonphotosynthetic material (Liu *et al.*, 2019). The algorithm is based on Python 3 and uses the already classified leaf point clouds to reconstruct leaf surfaces through plane fitting constrained by the leaf size parameter.

Vicari *et al.* (2019) introduced a threshold based on the covariance matrix of neighborhood points to eliminate points with significant errors from the estimated LIAD. The algorithm is based on Python 2. It initially conducts the nearest neighbors search around every point in a leaf-only point cloud for nearby points that are then used in the estimation of leaf normals. The algorithm aims to balance between having several neighboring points small enough to avoid calculating angles from more than a single leaf and having an adequate number of points to decrease the effect of data noise (Vicari *et al.*, 2019).

Stovall *et al.* (2021) developed Terrestrial Laser Scanning Leaf Angle Function (TLSLeAF), an algorithm that calculates LIAD from gridded point clouds. The algorithm is based on the R language and has a built-in feature that classifies wood and leaves. TLSLeAF calculates leaf normals directly from the gridded TLS point clouds. The computation of the LIAD is with respect to

Table 1 An overview of the point cloud leaf inclination angle distribution (LIAD) estimation methods under study.

LIAD estimation method	Abbreviated name	Programming language	Wood/leaf separation	Leaf size
Bailey & Mahaffee (2017)	Bailey	C++	No	No
Liu *et al*. (2019)	Liu	Python	No	Yes
Stovall *et al*. (2021)	TLSLeAF	R	Yes	No
Vicari *et al*. (2019)	Vicari	Python	No	No
Zheng & Moskal (2012)	Zheng	C++	No	No
Point Cloud Library (n.d.)	PCL	C++	No	No

the horizon in the point cloud grid directly from the leaf surface normals (Stovall *et al*., 2021).

Kuusk (2020) used Point Cloud Library (PCL) – a standalone, large-scale, open-source project designed for the purpose of processing 2D/3D images and point clouds (Point Cloud Library, n.d.). Given a geometric surface, the Point Cloud Library's normals estimation feature directly computes surface normals at each point in the cloud (Point Cloud Library, n.d.).

Table 1 summarizes the publications and their corresponding abbreviated names, which will be used as references throughout the following text for conciseness.

Data

Both real tree data obtained from terrestrial LiDAR scans and simulated LiDAR data from synthetic 3D tree models were used for the TLS algorithms' evaluation. The performance of TLS-based algorithms was also evaluated against the established non-TLS-based LDP approach (Ryu *et al*., 2010; Pisek *et al*., 2011) that used images of the same target canopy as an input.

TLS field data TLS point clouds for four trees from the Kumpula Botanic Garden, Helsinki, Finland (60.202°N, 24.955°E), were collected on October 12, 2021, using a Leica P40 Scan Station. This scanner has a laser with a 1550 nm wavelength and a beam divergence of 0.23 milliradians (mrad). The trees of interest were scanned from four different positions with a scan resolution of 0.018° (0.31 mrad). They included common pear (*Pyrus communis* L. *'Olga'*), European oak (*Quercus robur* L.), Himalayan rosebay (*Rhododendron* cf. *brachycarpum*), and European beech (*Fagus sylvatica* L.). LiDAR data for four additional trees from the Royal Botanic Gardens at Kew, United Kingdom (51.478°N, 0.295°W), were acquired on October 17, 2017, using a 3D RIEGL VZ-400 portable laser scanner. This scanner operates at a 1550 nm wavelength and a beam divergence of 0.35 mrad. An angular resolution of 0.04° was used. Both scanners in this study use the time-of-flight principle to measure the distance to a target. At both Kumpula and Kew, a tripod was used to support the scanner at a position that was 1.5 m above the ground, and measurements were taken from four different positions in a cross pattern, roughly 5 m from each tree. Individual tree species that were scanned at Kew included a date plum (*Diospyros lotus* L.), the maidenhair tree (*Ginkgo biloba* L.), the Japanese hop hornbeam (*Ostrya japonica* Sarg.), and the Wollemi pine (*Wollemia nobilis* W.G.Jones, K.D.Hill & J.M.Allen). Fig. 1(a–h) offers an overview of the scanned trees from Kumpula and Kew. It shall be noted that all trees were scanned in mid-October during the senescent period, and as such, might not provide LIAD type that would be expected or considered typical for these species during the main growing period.

Simulated TLS data 3D synthetic tree models were generated using Arbaro, an open-source software based on geometrical observables to produce and style three-dimensional canopies for replicating natural scenery (Weber & Penn, 1995). The three artificial trees, roughly following three different leaf inclination angle distribution types (spherical, uniform, erectophile), were further edited in Blender v.3.4 (Foundation, n.d.). Helios, a three-dimensional (3D) plant and environmental modeling framework (Bailey, 2019) was used to generate simulated LiDAR data of the three synthetic canopies. The simulated data was generated through a rectangular scan pattern, with the number of scan points in the zenithal direction set to 5000 and 9000 in the azimuthal direction. The minimum and maximum scan zenithal angles were set at 30° and 130°; the minimum and maximum scan azimuthal angles were set at 0° and 360°. Simulations were run with a beam radius of 0, such that only one return per pulse was possible. Positioned 1.5 m above the ground, the virtual scanner captured measurements from four equidistant positions surrounding each synthetic tree. The simulated canopies are shown in Fig. 1(i–k).

Leveled digital photography field data The leveled digital images were taken under calm conditions to minimize the effects of wind on leaves (Tadrist *et al*., 2014). The cameras used were an Apple iPhone SE 2020 with a 12-megapixel f/1.8 aperture wide camera and a Sony Xperia Z5 Compact phone with a 23-megapixel 1/2.3-inch multi-aspect BSI CMOS sensor, along with an F2.0 lens, both hand-balanced (based on the observer's judgment). The leveled images of the canopy were taken in all azimuth directions and at different heights of the canopy using a ladder if needed. The number of images taken varied from 5 (*Rhododendron* cf. *brachycarpum*) to 37 (*Quercus robur*), depending on the height and size of each tree. Following Pisek *et al*. (2013), at least 75 leaf inclination angle measurements must be collected from the image dataset to obtain a statistically representative sample for characterizing the leaf inclination angle distribution of each tree. Measuring the leaf inclination angle involves identifying the leaf plane, from which the leaf normal is determined. Leaves were chosen based on their orientation, ensuring they were approximately parallel to the camera's viewing direction. The angles of the selected leaves were then measured using the 'angle measurement tool' in the freeware program ImageJ (http://rsbweb.nih.gov/ij/). Pisek *et al*. (2011) provide more information on the leaf inclination angle retrieval with the LDP

New Phytologist

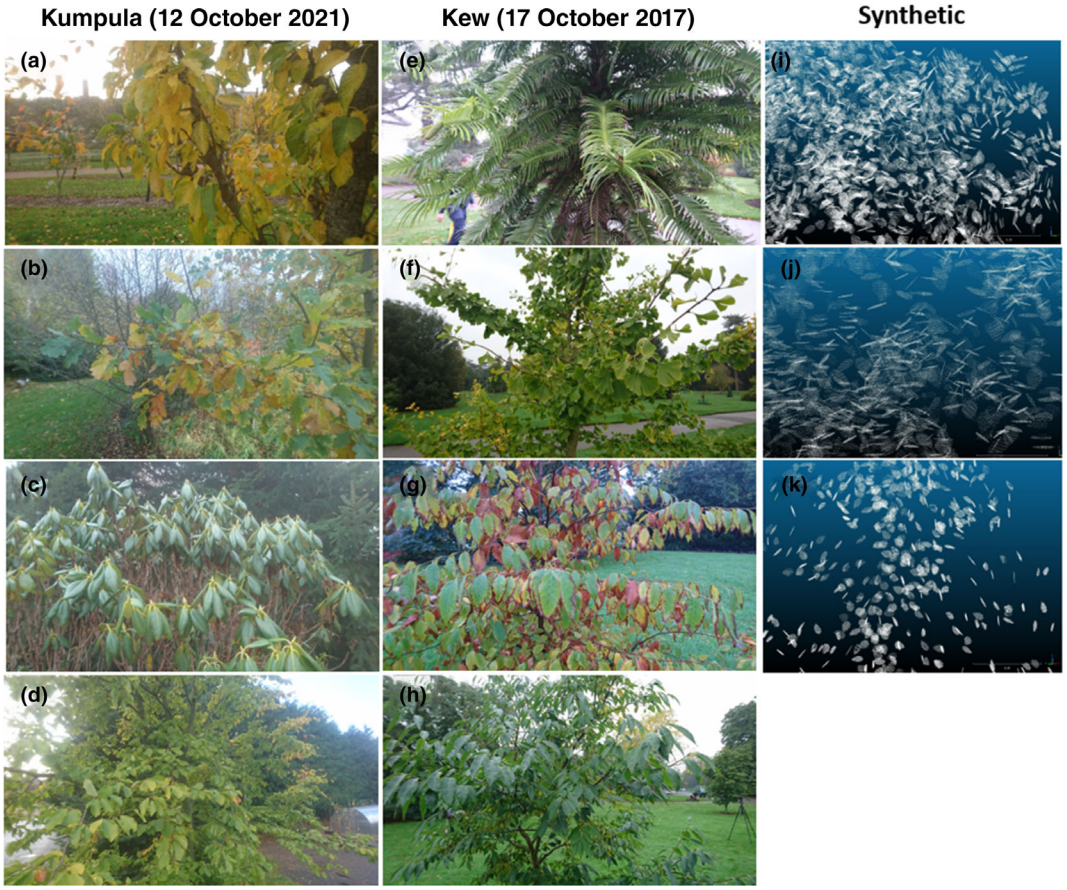

Fig. 1 Pictures of the tree representations included in this study: (a) *Pyrus communis* '*Olga*', (b) *Quercus robur*, (c) *Rhododendron* cf. *brachycarpum*, (d) *Fagus sylvatica*, (e) *Wollemia nobilis*, (f) *Gingko biloba*, (g) *Ostrya japonica*, (h) *Diospyros lotus*; synthetic (i) spherical, (j) uniform, and (k) erectophile point clouds.

approach. Fig. 1 includes examples of leveled digital photographs for each species included in this study.

Data pre-processing First, filtering of scans from the Riegl VZ-400 instrument was performed using the RiSCAN Pro software (RIEGL Laser Measurement Systems GmbH, Horn, Austria) to remove noisy points from the real LiDAR data and retain only high-confidence range values based on the pulse shape deviation (Pfennigbauer & Ullrich, 2010). Scans from the Leica instrument were processed in Leica Cyclone (v.9.4.0), using a similar but proprietary filter. Co-registration was conducted to align the multiple scans using five artificial targets that were placed throughout the scene. The trees of interest were manually extracted from the co-registered point clouds using the CloudCompare software. The TLS data was further prepared based on the specific requirements of each LIAD estimation algorithm. Individual scans for each tree were exported from RiSCAN PRO and Leica Cyclone as gridded TLS scan point clouds (PTX format), an input file format required for the TLSLeAF algorithm (Stovall *et al.*, 2021). Second, individual scans were exported into an American Standard Code for Information Interchange (ASCII) file format (.XYZ), and parameters for each scan were specified in a separate metadata file to facilitate data processing for the method proposed by Bailey & Mahaffee (2017). Individual TLS scans for each tree were merged for the following approaches: Zheng & Moskal (2012), Vicari *et al.* (2019), Liu *et al.* (2019) and the Point Cloud Library. The merged scans were also converted into the PCD (Point Cloud Data) file format, specifically for the Point Cloud Library.

Leaf-wood separation The TLSLeAF algorithm has an inbuilt feature that separates leaves from wood using supervised classification (random forest) based on multiscale normal estimates (Stovall *et al.*, 2021). However, with the other algorithms not possessing a similar feature, the leaf-wood separation of the real TLS scans was conducted using a Python package called TLSeparation for other algorithms except TLSLeAF. The TLSeparation package is a leaf-wood classification package for TLS data that performs unsupervised classification based on geometric features and shortest path analysis (Vicari, 2017). Leaves were separated from the wood in the synthetic, simulated 3D objects using 'Aspose.3D' assets extractor (Aspose.3D Product Family, n.d.), an open-source application used to separate embedded meshes and textures from OBJ files.

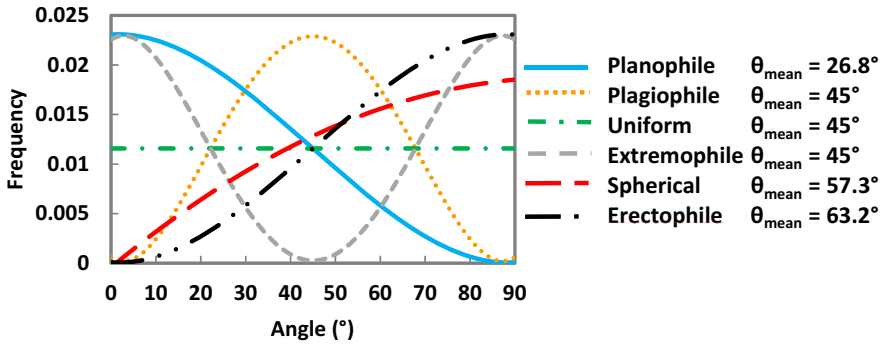

Fig. 2 The six classical predefined mathematical functions by De Wit (1965).

Estimation of leaf inclination angles TLSLeAF, Liu, and Vicari provide the LIA information directly, while the output of the other algorithms is leaf normal vectors. Leaf normal vectors were converted into leaf inclination angles (in degrees) with Eqn 1:

$$\alpha = \cos^{-1}\left|\vec{N}.\vec{z}\right| \times \frac{180}{\pi} \quad \text{Eqn 1}$$

where $\vec{N}$ represents the unit normal vector and $\vec{z}$ is the unit zenith vector.

Benchmarking of algorithms Estimation of leaf inclination angles using TLS-based algorithms was performed on a Lenovo Thinkpad P15s Gen 1 laptop equipped with an Intel(R) Core i7-10610U CPU @ 1.80 GHz 2.30 GHz processor. This machine had Windows 10 Pro 64 and Ubuntu Linux LTS (v.20.04) operating systems. The laptop featured a maximum memory capacity of 48 GB 2667 MHz DDR4-2666 RAM and 512 GB solid-state drive (SSD) storage. The computing setup had both a dedicated graphics card and integrated graphics. It included a 2 GB NVIDIA Quadro P520 graphics card, as well as Intel UHD Graphics. Five algorithms were tested within the Windows operating system during the leaf inclination angle estimation process, while the PCL algorithm was executed on the Ubuntu Linux LTS system.

Leaf inclination angle distribution The resulting leaf inclination angles from the algorithms were fitted with the two-parameter Beta distribution function (Goel & Strebel, 1984). This function was reported as best suited for the description of the probability distribution function (PDF) of the leaf inclination angle distribution (Wang *et al.*, 2007).

The distribution of leaf inclination angles can be described using the six common functions proposed by De Wit (1965) that are based on empirical evidence and mathematical considerations (Raabe *et al.*, 2015; Chianucci *et al.*, 2018). These functions include uniform, planophile, plagiophile, erectophile, extremophile, and spherical (Fig. 2). Uniform canopies have an equal proportion of leaf inclination angles at any angle; planophile canopies are dominated by horizontally oriented leaves; plagiophile canopies are dominated by leaves most frequent at an oblique inclination; erectophile canopies are dominated by vertically oriented leaves; extremophile canopies have a high frequency of both horizontally and vertically oriented leaves, and in spherical canopies, the relative frequency of leaf inclination angles is the same as that for surface area elements of a sphere (Lemeur & Blad, 1974).

The classical distributions are extensively utilized and offer a more straightforward interpretation than the beta distribution's parameter values. The measured distributions of leaf inclination angles ($f(\theta_L)$) were categorized by identifying the most similar classical distribution type. To calculate the difference from the distributions proposed by De Wit (1965) $f_{\text{deWit}}(\theta_L)$, a modified inclination index, developed by Ross (1975), was applied to each leaf inclination angle distribution:

$$\chi_L = \min \int_0^{\pi/2} \left|f(\theta_L) - f_{\text{de Wit}}(\theta_L)\right| d\theta_L \quad \text{Eqn 2}$$

The measured LIADs were then assigned to the class that returned the lowest X_L score.

Statistical analysis Statistical tests were carried out to assess the level of agreement between the leaf inclination angle distributions obtained from the five TLS algorithms, as well as the reference LDP approach. With the algorithms potentially predicting a variety of LIAD types, the tests were conducted using the Mann–Whitney *U*-test, a nonparametric test that does not assume that the data have a particular distribution, such as a normal distribution (McKnight & Najab, 2010). The tests were executed using RStudio 2022.07.2 (RStudio, Boston, MA, USA). Pair-wise matrices were generated to facilitate inter-comparison between the algorithms.

Additionally, a comparative analysis was performed on the LIAD of the synthetic model with the LIAD obtained from each approach using the simulated point clouds at 5-degree intervals. To achieve this, a normality test was performed at each 5-degree interval to assess the distribution of the data. If the data were found to be normally distributed, a parametric *t*-test was conducted. Conversely, a nonparametric Mann–Whitney *U*-test was used if the data were not normally distributed.

Results

LIAD estimation from real trees

Tables 2 and 3 provide the statistical moments for the obtained leaf inclination angle distributions by the individual algorithms for real, nonsimulated trees. Tables 4 and 5 present the results of

New Phytologist

Table 2 Statistical moments (i.e. average leaf inclination angle (ALIA), SD (SD), two parameters μ, ν, number of observations (*n*)) of the leaf inclination angle measurements and the leaf inclination angle distribution (LIAD) function type, after de Wit (1965) from the evaluated LIAD approaches on the Kumpula Botanical Garden species.

Method	ALIA	SD	μ	ν	Type	*n*
Pyrus communis 'Olga'						
Bailey	54.4	22.9	1.07	1.63	S	2 123 805
Liu	71.41	19.72	0.5	1.91	E	5 082 338
PCL	69.55	16.68	0.93	3.18	E	5 082 520
TLSLeAF	55.72	19.31	1.57	2.55	S	4 003 057
Vicari	63.39	19.7	0.99	2.36	E	783 775
Zheng	67.47	17.73	0.96	2.87	E	5 083 496
LDP	68.69	20.05	0.62	2.01	E	78
Quercus robur						
Bailey	53.9	21.9	1.21	1.81	S	1 758 678
Liu	59.31	26.33	0.55	1.07	S	5 140 721
PCL	57.01	20.84	1.22	2.11	S	5 139 379
TLSLeAF	52.2	19.56	1.74	2.41	S	3 728 297
Vicari	58.44	20.35	1.21	2.24	S	1 925 924
Zheng	58.2	20.62	1.19	2.17	S	5 150 274
LDP	51.19	21.47	1.43	1.88	S	129
Rhododendron cf. *brachycarpum*						
Bailey	52.52	23.3	1.09	1.53	S	1 496 228
Liu	65.77	21.29	0.68	1.84	E	3 752 621
PCL	61.58	17.12	1.57	3.4	E	3 752 471
TLSLeAF	57.71	18.95	1.5	2.69	S	3 998 834
Vicari	60.17	19.1	1.3	2.62	E	864 441
Zheng	63.21	17.77	1.3	3.07	E	3 753 702
LDP	53.1	17.22	2.3	3.31	S	86
Fagus sylvatica						
Bailey	54.5	22	1.18	1.81	S	3 409 205
Liu	60.79	24.74	0.62	1.28	S	9 286 541
PCL	57.83	19.04	1.48	2.66	S	9 286 334
TLSLeAF	54.21	19.1	1.72	2.6	S	8 997 463
Vicari	57.44	18.81	1.55	2.73	S	2 632 255
Zheng	59.66	19.17	1.32	2.6	S	9 294 361
LDP	48.47	17.05	2.73	3.19	PG	125

E, erectophile; PG, plagiophile; S, spherical.

the Mann–Whitney *U*-test for the six TLS algorithms and the LDP approach. The null hypothesis was that the leaf inclination angle distributions (LIADs) of the compared pair of algorithms are not different from each other. The test was carried out at a significance level of 0.05. If the *P*-value is less than the significance level, we conclude there is a statistically significant difference between the LIADs of the compared pair of algorithms.

In Kumpula (Table 4), significant contrasting outcomes were observed between Bailey and PCL regarding the LIAD of the *Pyrus communis* '*Olga*' tree. Similarly, the Liu algorithm exhibited significant disagreement with Bailey, TLSLeAF, and Vicari while aligning with the remaining methods. The LDP method was not significantly different from all TLS algorithms except for Bailey ($P = 0.003$) and TLSLeAF ($P = 0.036$). For the estimation of LIAD in *Quercus robur*, all approaches displayed agreement, with Liu being significantly different from all methods except Vicari and Zheng. Both *Rhododendron* cf. *brachycarpum* and *Fagus sylvatica* cases demonstrated similar outcomes, where all LIAD estimation methods showed no statistically significant differences, with the exception of two cases in which the Liu algorithm disagreed with Bailey. The reference LDP approach was generally consistent with the TLS approaches except for *Fagus sylvatica*, where it indicated a different LIAD type (plagiophile) than the TLS methods (spherical) (Table 2).

For the Kew garden's species, all LIAD estimation methods agreed on the LIAD of the *Wollemia nobilis*, except for the Liu algorithm, which was found significantly different from the rest (Table 5). Remarkably, no statistically significant difference was observed for the LIAD estimation of the *Ginkgo biloba* across all approaches, except where Liu and TLSLeAF were significantly different ($P = 0.027$). A similar outcome was observed for *Ostrya japonica*, mirroring the results of *Ginkgo biloba*, where results from all TLS algorithms were not statistically different except for two cases of Liu algorithm (Liu vs Bailey ($P = 0.039$) and Liu vs TLSLeAF ($P = 0.047$)). However, unlike with the *Ginkgo biloba*, the results from the LDP method were not significantly different from PCL, Vicari, and Zheng for the *Ostrya japonica*. For the LIAD estimation of *Diospyros lotus*, all TLS methods provided no significantly different results. The results for the LDP approach are significantly different from Bailey, TLSLeAF, and Liu. The

Table 3 Statistical moments (i.e. average leaf inclination angle (ALIA), SD (SD), two parameters μ, ν, number of observations (*n*)) of the leaf inclination angle measurements and the leaf inclination angle distribution (LIAD) function type, after de Wit (1965) from the evaluated LIAD approaches from the Royal Botanical Gardens at Kew.

Method	ALIA	SD	μ	ν	Type	*n*
Wollemia nobilis						
Bailey	46.45	23.04	1.36	1.45	U	453 603
Liu	45.4	27.16	0.86	0.88	U	744 902
PCL	45.43	21.88	1.6	1.63	U	746 278
TLSLeAF	49.74	21.79	1.44	1.78	S	1 084 722
Vicari	43.96	22.09	1.61	1.54	U	431 365
Zheng	46.49	22.34	1.48	1.58	U	746 409
LDP	46.71	22.05	1.52	1.64	U	80
Ginkgo biloba						
Bailey	56.95	21.96	1.07	1.84	S	317 708
Liu	63.8	22.65	0.66	1.6	S	550 153
PCL	64.27	18.29	1.13	2.82	E	550 787
TLSLeAF	50.89	21.46	1.44	1.88	S	592 273
Vicari	64.84	17.84	1.15	2.97	E	415 402
Zheng	63.92	18.45	1.13	2.77	E	550 809
LDP	57.67	18.9	1.52	2.7	S	78
Ostrya japonica						
Bailey	55.43	22.52	1.07	1.71	S	252 233
Liu	59.5	25.3	0.62	1.21	S	391 003
PCL	61.16	18.75	1.29	2.73	E	391 260
TLSLeAF	53.51	20.7	1.44	2.12	S	331 822
Vicari	62.18	18.65	1.23	2.75	E	245 306
Zheng	62.07	18.91	1.19	2.65	E	391 279
LDP	66.37	11.63	2.78	7.81	E	90
Diospyros lotus						
Bailey	50.73	20.21	1.69	2.18	S	238 516
Liu	52.76	21.61	1.33	1.88	S	479 766
PCL	52.45	16.72	2.52	3.52	PG	480 615
TLSLeAF	51.77	20.21	1.63	2.21	S	714 156
Vicari	51.95	16.09	2.8	3.83	PG	354 563
Zheng	52.93	16.98	2.39	3.41	PG	480 642
LDP	39.59	11	8.68	6.82	PG	100

E, erectophile; PG, plagiophile; S, spherical; U, uniform.

DLP approach also showed very different average leaf inclination angle (ALIA) (difference > 10°) and SD values compared to all TLS algorithms in the case of *Diospyros lotus* (Table 3).

LIAD estimation from simulated tree representations

The assessment and comparison of various LIAD estimation approaches using simulated tree representations of three different LIAD types (spherical, uniform, and erectophile) provided a further evaluation of the performance and agreement of the approaches with the corresponding synthetic models. Most of the techniques demonstrated comparable estimates of the ALIA, SD (Table 6), and PDFs (Fig. 3) within an acceptable range of the synthetic model's output for the simulated spherical LIAD tree representation. This finding suggests that these approaches effectively captured the spherical LIAD characteristics. The statistical analysis further supported this conclusion, with the tests indicating no statistically significant difference between the algorithms and the synthetic model (Table 7).

The synthetic uniform LIAD tree representation presented a wider range of ALIA values by the LIAD estimation methods compared to the spherical model (Table 6). Despite visible variation in obtained PDFs (Fig. 3), all algorithms displayed no significant difference ($P > 0.05$) from the synthetic uniform model and demonstrated agreement in identifying this LIAD type (Table 6).

The *P*-value results of the synthetic erectophile LIAD tree representation with steeper leaf inclination angles revealed that all the evaluated LIAD estimation approaches exhibited no statistically significant difference from the synthetic model (Table 7).

The comparative analyses at 5-degree intervals conducted between the synthetic LIAD models and each LIAD estimation method facilitated further evaluation of the performance and accuracy of these methods across different angle intervals. Algorithms mostly exhibited statistically significant differences in specific angle ranges, indicating deviations from the model (Fig. 4). The analysis with the uniform synthetic model revealed differences between the LIAD estimation methods and the model (Fig. 4g–l), suggesting a more limited capability of most of the methods in accurately estimating more horizontally aligned LIADs. Only Bailey's algorithm provided a LIAD distribution that followed the pattern of the prescribed synthetic uniform

New Phytologist

Table 4 Pair-wise comparison of *P*-values from the Mann–Whitney *U*-test for trees in Kumpula.

	Bailey	PCL	TLSLeAF	Vicari	Zheng	Liu	LDP
Pyrus communis 'Olga'							
Bailey	1.000						
PCL	**0.034**	1.000					
TLSLeAF	0.381	0.115	1.000				
Vicari	0.568	0.250	0.78	1.000			
Zheng	0.126	0.640	0.296	0.523	1.000		
Liu	**0.000**	0.865	**0.003**	**0.043**	0.400	1.000	
LDP	**0.003**	0.703	**0.036**	0.203	0.813	0.431	1.000
Quercus robur							
Bailey	1.000						
PCL	0.401	1.000					
TLSLeAF	0.374	0.978	1.000				
Vicari	0.463	0.684	0.688	1.000			
Zheng	0.449	0.709	0.722	0.851	1.000		
Liu	**0.006**	**0.048**	**0.044**	0.102	0.088	1.000	
LDP	0.728	0.371	0.353	0.432	0.427	**0.004**	1.000
Rhododendron cf. *brachycarpum*							
Bailey	1.000						
PCL	0.974	1.000					
TLSLeAF	0.416	0.827	1.000				
Vicari	0.578	0.863	0.796	1.000			
Zheng	0.885	0.885	0.863	0.878	1.000		
Liu	**0.014**	0.576	0.184	0.252	0.596	1.000	
LDP	0.646	0.849	0.756	0.869	0.854	0.319	1.000
Fagus sylvatica							
Bailey	1.000						
PCL	0.472	1.000					
TLSLeAF	0.412	0.724	1.000				
Vicari	0.479	0.960	0.711	1.000			
Zheng	0.555	0.807	0.675	0.805	1.000		
Liu	**0.026**	0.230	0.143	0.232	0.309	1.000	
LDP	0.667	0.756	0.703	0.756	0.811	0.437	1.000

Significantly different values are in bold.

model. In the analysis with the erectophile LIAD synthetic model, all algorithms consistently agreed with the model, but still with significant differences observed for most of the angle intervals. However, the algorithms still showed a reasonable match with the model over most of the LIAD range (Fig. 4m–r).

Processing time requirements

The TLS algorithms demonstrated varying processing times for estimating the LIAD. While the processing times differed among the algorithms, they were consistent across all point clouds that were analyzed. As an example, we report the processing times for the *Rhododendron* cf. *brachycarpum* point cloud, made of 3 753 702 data points from four scan positions (Table 8). The results reported in Table 8 correspond to the processing done on the Lenovo ThinkPad P15s Gen 1 laptop with a Core i7 CPU (full specifications in 'Benchmarking of algorithms' in the Materials and Methods section). The Bailey method exhibited the fastest processing time for LIAD estimation. The Zheng algorithm exhibited the second fastest time. TLSLeAF exhibited the third fastest processing time for LIAD estimation, processing each individual point cloud separately before the overall LIAD was obtained. This performance confirms the rapid processing as originally reported by Stovall *et al.* (2021). Vicari and PCL methods followed, respectively, where each algorithm efficiently estimated the LIAD while still maintaining reasonable processing times (under 5 min). The Liu algorithm required close to 44 min to fully process the data. The algorithms are implemented in different programming languages, which impacts the processing speed. We tested the algorithms in the way they are distributed. Relative efficiency gains could be obtained by implementing algorithms in different programming languages.

Discussion

The LIAD estimation approaches used in this study demonstrated both strengths and weaknesses. These strengths and weaknesses were assessed based on various aspects, including setup, input data formats, LIAD estimation procedures, and overall performance in the conducted tests. In this section, we will consider the pros and cons of each method, as well as some of the challenges, before summarizing overall recommendations.

The Bailey algorithm involves a relatively complex setup procedure; however, its detailed documentation and available

Table 5 Pair-wise comparison of *P*-values from the Mann–Whitney *U*-test for trees in Kew.

	Bailey	PCL	TLSLeAF	Vicari	Zheng	Liu	LDP
Wollemia nobilis							
Bailey	1.000						
PCL	0.148	1.000					
TLSLeAF	0.117	0.541	1.000				
Vicari	0.175	0.652	0.401	1.000			
Zheng	0.221	0.449	0.293	0.616	1.000		
Liu	**0.013**	**0.028**	**0.031**	**0.024**	**0.019**	1.000	
LDP	0.237	0.724	0.429	0.865	0.538	**0.026**	1.000
Ginkgo biloba							
Bailey	1.000						
PCL	0.761	1.000					
TLSLeAF	0.561	0.692	1.000				
Vicari	0.671	0.994	0.606	1.000			
Zheng	0.818	0.974	0.745	0.999	1.000		
Liu	0.074	0.829	**0.027**	0.958	0.763	1.000	
LDP	0.588	0.974	0.439	0.887	0.999	0.219	1.000
Ostrya japonica							
Bailey	1.000						
PCL	0.737	1.000					
TLSLeAF	0.679	0.698	1.000				
Vicari	0.881	0.872	0.831	1.000			
Zheng	0.899	0.860	0.851	0.978	1.000		
Liu	**0.039**	0.508	**0.047**	0.654	0.630	1.000	
LDP	**0.027**	0.092	**0.034**	0.097	0.091	**0.031**	1.000
Diospyros lotus							
Bailey	1.000						
PCL	0.745	1.000					
TLSLeAF	0.851	0.745	1.000				
Vicari	0.910	0.878	0.901	1.000			
Zheng	0.692	0.887	0.703	0.865	1.000		
Liu	0.427	0.735	0.419	0.903	0.686	1.000	
LDP	**0.028**	0.107	**0.029**	0.135	0.093	**0.021**	1.000

Significantly different values are in bold.

tutorials greatly facilitate the setup procedure. The method does not account for differentiating between wood and leaves (Bailey & Mahaffee, 2017). It compensates for the bias introduced by the scanner position in estimating leaf inclination angles (Bailey & Mahaffee, 2017). This compensation is achieved through separate scans for each scan position, saved in an ASCII file format, and an accompanying XML file specifying scan parameters (such as scanner position, resolution, and intensity). Bailey & Mahaffee (2017) mention that the algorithm was found to be minimally impacted by variations in scan resolution. It is possible that the small observed discrepancies in this study could be influenced by the relatively low-density areas of the single low-resolution scans used with the algorithm. Overall, the algorithm demonstrated consistency in agreement with other TLS approaches. The comparative analysis was conducted at 5-degree intervals using high-resolution synthetic point clouds (Fig. 4) confirmed the Bailey algorithm's superior performance due to weighting each normal vector, mitigating bias towards normal vectors that face the TLS scanner (Bailey & Mahaffee, 2017), which is currently not done by the other algorithms included in this intercomparison.

The Liu algorithm stands out for its comparatively simpler setup process, requiring the establishment of a Python 3 environment and specifying the leaf constraint and input point cloud location. The input point cloud for each tree follows the widely used ASCII format (Pepe *et al.*, 2016). In contrast to the Bailey approach, the Liu algorithm requires an extra step since it generates LIAD information by using point clouds generated from merging co-registered individual scans to increase point density (Liu *et al.*, 2019). While the method recognizes the importance of differentiating leaves from woody material, it does not possess this feature by default. The original study employed a Support Vector Machine classification technique to separate leaves from wood. The algorithm's consistency with the ALIA values of other TLS algorithms is notable. However, it exhibited poor performance when fitting the beta distribution, with distinct differences in patterns compared to the other algorithms, where the algorithm consistently overestimated leaf inclination close to the extreme value of 90° (Fig. 3a–c). It's estimated ALIA or SD values tended to be higher than those of other algorithms in most cases. The performance of the algorithms might also have been undermined by a wide variation in leaf sizes and shapes of the sampled real trees. The Liu algorithm performed relatively well in the case of the synthetic point clouds, where the leaf size and shape did not vary. The Liu algorithm managed to identify the

New Phytologist

Table 6 Statistical moments (i.e. average leaf inclination angle (ALIA), SD, two parameters μ, ν, number of observations (*n*)) of the leaf inclination angle measurements and the leaf inclination angle distribution (LIAD) function type, after de Wit (1965) from the evaluated LIAD approaches for the synthetic tree models.

Method	ALIA	SD	μ	ν	Type	*n*
Spherical						
Synthetic	56.86	21.65	1.11	1.91	S	7908
Bailey	58.32	21.74	1.02	1.88	S	4 625 486
Liu	60.79	21.11	0.97	2.02	S	3 032 461
PCL	60.85	21.24	0.95	1.98	S	3 023 816
Vicari	60.65	21.04	0.99	2.04	S	3 021 288
Zheng	60.62	21.05	0.99	2.03	S	3 047 628
LDP	52.16	22.62	1.2	1.66	S	231
Uniform						
Synthetic	39.72	25.03	1.22	0.97	U	14 296
Bailey	42.03	25.65	1.1	0.96	U	3 907 867
Liu	46.69	26.35	0.92	0.99	U	2 568 545
PCL	45.94	26.03	0.97	1.01	U	2 557 428
Vicari	45.65	25.87	1	1.03	U	2 471 292
Zheng	45.98	25.72	1.01	1.05	U	2 584 099
LDP	39.56	22.69	1.61	1.26	U	229
Erectophile						
Synthetic	66.38	16.64	1.22	3.44	E	1351
Bailey	68.44	15.22	1.29	4.09	E	1 374 498
Liu	69.19	15.6	1.14	3.78	E	874 461
PCL	69.2	15.61	1.13	3.77	E	875 206
Vicari	69.15	15.56	1.15	3.8	E	874 350
Zheng	69.15	15.57	1.15	3.8	E	875 966
LDP	64.8	17.96	1.14	2.92	E	205

E, erectophile; S, spherical; U, uniform.

correct LIAD types, although some erroneous patterns were evident towards extreme values of leaf inclination angles. The Liu algorithm was still able to predict a very similar PDF to other algorithms using the synthetic erectophile model, as the comparative analysis conducted at 5-degree intervals revealed.

TLSLeAF is a user-friendly open-source algorithm that can be set up by cloning its R source code from the associated GitHub account and ensuring the installation of the required dependency, a point cloud processing software (Cloud Compare). However, the algorithm's gridded input data format differs from the widely used ASCII file formats. Converting existing ASCII files into the PTX or similar gridded data formats can be challenging. The PTX format, on the other hand, offers valuable individual scan information such as point cloud size, transformation parameters, scanner position, intensity, and more. Like the Bailey algorithm, the PTX format allows for the consideration of scanner position bias in estimating LIAD without requiring a separate file for scan metadata. TLSLeAF distinguishes itself from other algorithms by offering an inherent feature for separating leaves from wood (Stovall *et al.*, 2021). This additional capability gives TLSLeAF a theoretical advantage, eliminating the need for external methods or techniques to differentiate between these components. It shall be noted that this study did not evaluate the performance of this leaf-wood separation feature. In terms of performance, a notable limitation arose in its ability to accurately predict LIAD types that departed from the spherical case. Despite this limitation, TLSLeAF remains an accessible, convenient algorithm for LIAD estimation, with a straightforward setup process. Further exploration and improvement are recommended and may be needed to enhance its capability to predict a wider range of LIAD types.

The PCL, Vicari, and Zheng algorithms provided the mutually most consistent, not significantly different distributions, very similar statistical moments, as well as identifying the same deWit leaf inclination distribution type in all scenarios as well. The PCL algorithm requires a complex setup process, even when using its prebuilt binaries designed for different operating systems. Following Kuusk (2020), a Linux environment was chosen to execute the algorithm. The algorithm relies on merged ASCII point clouds, which serve as the precursor to the PCD format, the designated input data format for PCL. Overall, the PCL algorithm showcased robust and reliable performance for most of the studied cases, consistently producing results that aligned closely with other TLS algorithms. The setup process for the Python 2-based Vicari algorithm requires linking modules and obtaining the necessary dependencies. However, similarly to the Liu and PCL algorithms, Vicari utilizes simple, merged ASCII format point clouds as input data. Using simulated datasets highlighted the algorithm's good performance. Despite its somewhat complicated setup process, the Vicari algorithm proved reliable and effective for LIAD estimation.

The setup process for the Zheng algorithm requires older versions of dependencies such as Visual Studio 2015 update 3, boost 1.60.0, Eigen3, and CGAL 4.11.1, which may pose challenges

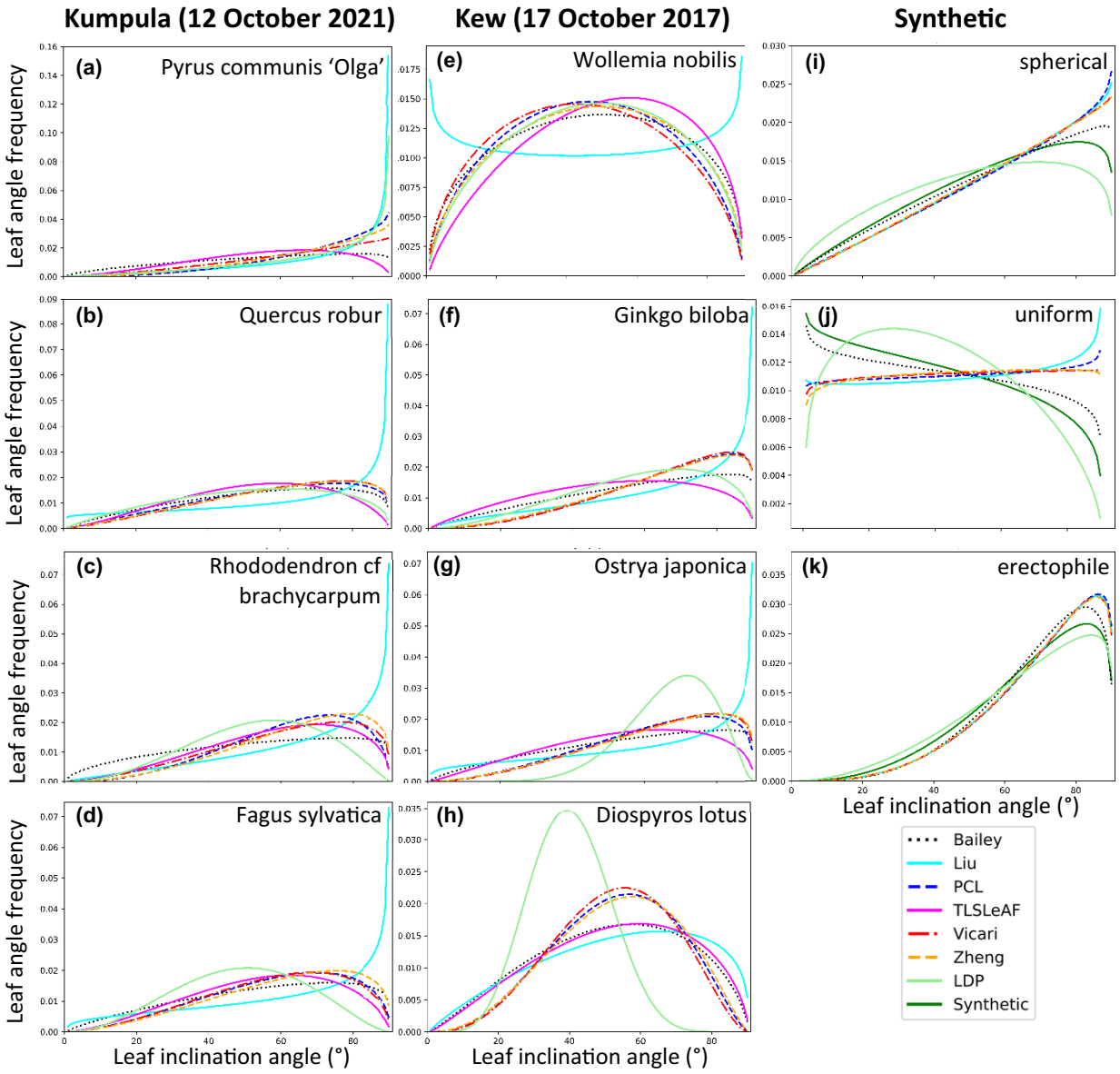

Fig. 3 Fitted beta distributions of leaf inclination angles for the tree representations included in this study: (a) *Pyrus communis 'Olga'*, (b) *Quercus robur*, (c) *Rhododendron* cf. *brachycarpum*, (d) *Fagus sylvatica*, (e) *Wollemia nobilis*, (f) *Gingko biloba*, (g) *Ostrya japonica*, (h) *Diospyros lotus*; synthetic (i) spherical, (j) uniform, and (k) erectophile point clouds.

Table 7 *P*-value results of LIAD estimation approaches against the synthetic spherical, uniform, and erectophile LIAD tree representations.

Method	Spherical	Uniform	Erectophile
Bailey	0.903	0.419	0.825
Liu	0.863	0.193	0.777
PCL	0.803	0.177	0.773
Vicari	0.929	0.171	0.782
Zheng	0.938	0.188	0.782
LDP	0.399	0.137	0.898

when integrating them into the latest computing environments. Similar to the Liu, PCL, and Vicari algorithms, the Zheng algorithm uses co-registered and merged point clouds in the widely used ASCII format for LIAD estimation. It does not include a feature for leaf-wood separation. Like other algorithms except Bailey, it encountered challenges when estimating the simulated, synthetic uniform LIAD type.

It should be noted that errors in estimating the LIAD tend to decrease with increasing scan density (Bailey & Mahaffee, 2017). Some single scans may exhibit a lower density of points, impacting the quality of LIAD estimation. Most methods in this study overcome this limitation by using merged scans to increase the overall point density. TLSLeAF addresses density measurement bias by calculating statistics of angle measurements within voxels and reconstructing the distribution of measurements using an equal number of simulated angles (Stovall *et al.*, 2021). Despite

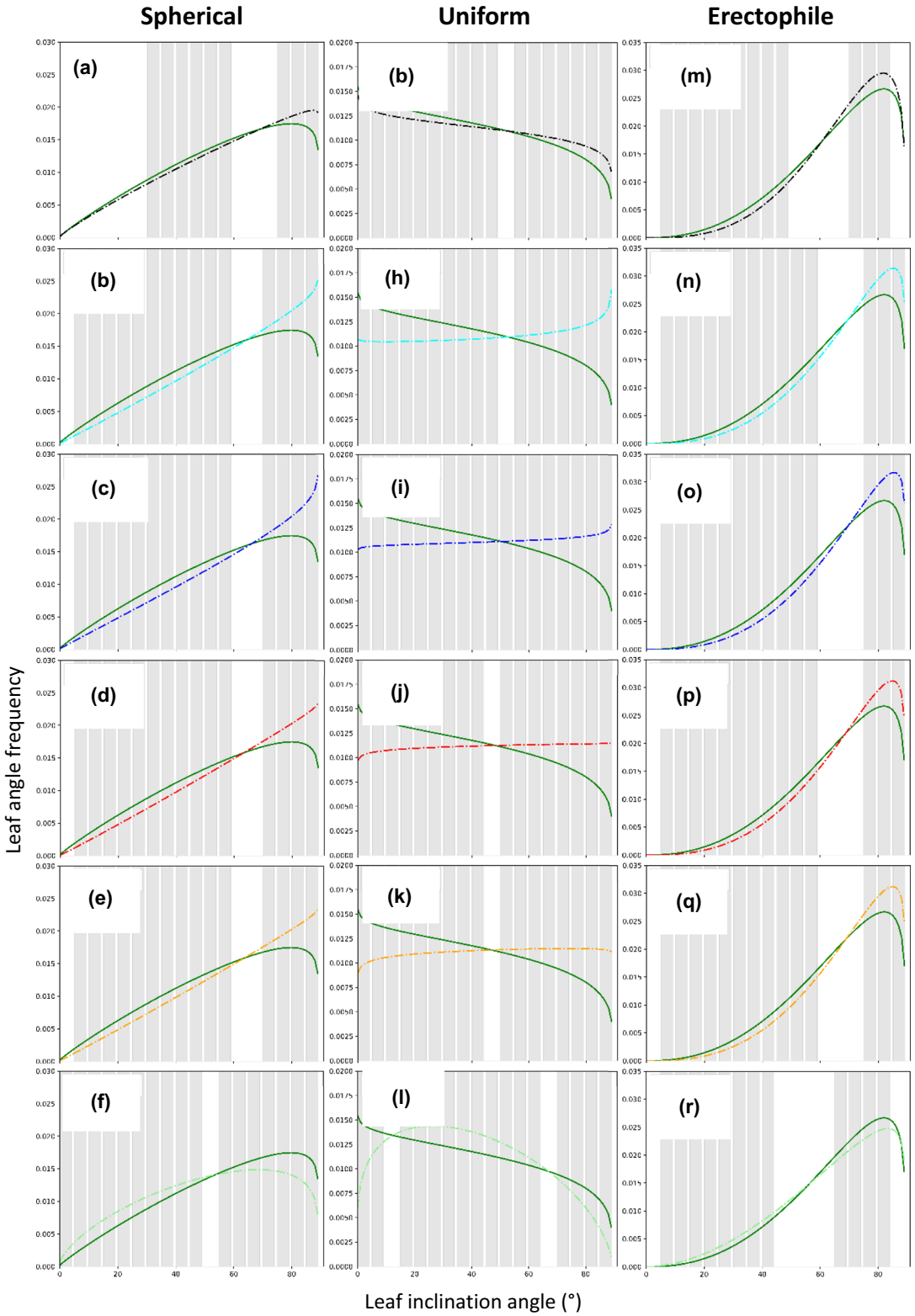

Fig. 4 *P*-value results of leaf inclination angle distribution (LIAD) estimation approaches against the synthetic spherical, uniform, and erectophile LIAD tree representations (green solid lines). Gray bars mark significant differences at the 0.05 level. Bailey (a, g, m), Liu (b, h, n), PCL (c, i, o), Vicari (d, j, p), Zheng (e, k, q), and LDP (f, l, r).

Table 8 Ranking of TLS LIAD estimation methods based on their processing durations for the *Rhododendron* cf. *brachycarpum* point cloud.

Rank	Method	Processing speed
1	Bailey	1 min[1]
2	Zheng	1 min 32 s[1]
3	TLSLeAF	1 min 56 s
4	Vicari	4 min 32 s
5	PCL	4 min 43 s[1]
6	Liu	43 min 42 s

[1]Symbol marks normal estimation only.

Table 9 Overview of major advantages and disadvantages of included TLS methods in this study.

Algorithm	Advantage	Disadvantage
Bailey	Superior performance across different LIAD types; compensates for the bias introduced by the scanner position in estimating leaf inclination angles	Complex setup process (but detailed documentation and tutorials available)
Liu	Simple setup process	Sensitivity to leaf size
TLSLeAF	In-built leaf-wood separation procedure; user-friendly open-source algorithm	Only PTX. format supported; limited sensitivity to a wider range of LIAD types
PCL, Vicari, Zheng	Consistent performance within this group of algorithms	Complex setup process

such measures, algorithms that utilize merged point clouds performed better than their single-scan counterparts in this study. This finding suggests the benefits of merging multiple scans to increase point density and enhance LIAD estimation accuracy could outweigh the concern for the bias introduced by the scanner position in estimating leaf inclination angles. This performance disparity emphasizes the need for further investigation into the choice of using either single or combined scans for LIAD estimation.

The LDP method was confirmed to be limited due to its manual, nonautomated selection of appropriate leaves for LIAD estimation, as previously noted by Vicari *et al.* (2019). Another limitation arises from the fact that the LDP approach may not always assess the entire profile of the canopy because of the limited means to reach and collect the photos higher in the canopy (but see McNeil *et al.*, 2016). The upper canopy levels often exhibit steeper leaf inclination angles, while the middle and bottom layers tend to have more horizontal and lateral growth directions (Niinemets, 2010). In the case of *Fagus sylvatica* in this study, the LDP method undersampled the steeper angles to be expected at the top of the canopy, leading to a lower proportion of these angles being represented by the approach. By contrast, TLS captures the entire height profile of a canopy (Moskal & Zheng, 2012), ensuring that the steeper leaves at the top are not missed. However, the LDP method offers the advantage of strictly utilizing photosynthetic material exclusively for LIAD estimation through manual leaf-by-leaf assessment. Another drawback of the LDP method is its limited accuracy in estimating LIAD for curved leaves (*Diospyros lotus* in our study). Despite these limitations, the LDP approach exhibited general consistency and compatibility with the TLS algorithms, mainly when the leaves exhibited minimal curvature. Although the TLS algorithms demonstrated superior LIAD estimations when a more significant proportion of leaf area was projected towards the scanner, closer to the synthetic spherical and erectophile models, the LDP approach demonstrated proficiency in estimating the synthetic uniform model. It obtained an ALIA value closest to the model, showcasing its competence in cases where leaf distribution is more horizontal and exhibits less curvature.

Study challenges

The study illustrated how well the various LIAD estimation approaches performed against each other. However, some challenges may have influenced the inter-comparison outcomes. These challenges are discussed below.

Leaf-wood separation A common tool was employed, with most methods lacking a built-in leaf-wood separation feature. As a result, the Liu, PCL, Vicari, and Zheng algorithms were tested using the same leaf-only point clouds. Similarly, the Bailey algorithm was tested with these leaf-only point clouds, but as individual scans. However, due to the TLSLeAF algorithm possessing its leaf-wood separation capability, its input consisted of the full, unseparated versions of the trees' point clouds. This discrepancy in leaf-wood separation between TLSLeAF and the other algorithms introduces a potential source of inconsistency in the inter-comparison of LIAD estimation methods, which may have compromised the accuracy of the evaluation when real point clouds were used. Leaf-wood separation methods themselves may have encountered challenges in accurately classifying leaves from wood. Different algorithms may also have different sensitivities to the wood-leaf separation outcomes, since they use varying criteria (such as the number of neighborhood points) to calculate the normals and leaf angles. However, the utilization of synthetic scans helped mitigate such discrepancies, as the meshes used to create the models were well-defined and known.

Input data file formats TLS algorithms commonly (four out of five in this study) use the ASCII file format. TLSLeAF employs the PTX file format or other gridded file formats. While the PTX format offers a higher level of scan information compared to a plain ASCII point cloud, it is not as widely adopted. The study encountered difficulties in generating PTX data for the synthetic data, which restricted the inclusion of TLSLeAF in this part of the intercomparison ('Simulated TLS data' in the Materials and Methods section). The choice of file format in TLS algorithms depends on various factors such as data requirements, compatibility with software tools, and specific project needs. While the ASCII format is commonly used, alternative formats like PTX may be preferred in some instances that demand more detailed scan information or specialized processing.

Recommendations

Analysis of real trees from the Kumpula and Kew Gardens' datasets revealed a high level of agreement among the TLS algorithms, indicating their general consistency and reliability. Nonetheless, the Liu and the TLSLeAF algorithms displayed preferences toward specific LIAD types, suggesting possible limitations in capturing the full range of different LIAD types.

Each LIAD estimation approach demonstrated both strengths and limitations (Table 9). The Bailey algorithm, despite its complex setup process, compensated for scanner position bias, which resulted in the best performance across different scenarios while exhibiting good consistency with other TLS approaches. Based on the results in our study, the Bailey algorithm may currently be the best TLS-based method to estimate LIAD in tree canopies. With its relatively simple setup process, the Liu algorithm showed discrepancies in frequency distribution patterns. In the case of TLSLeAF, further exploration and improvement are recommended and may be needed to enhance its capability to predict a wider range of LIAD types. Although the PCL algorithm required a complex setup process, it demonstrated very good performance and strong agreement with the other two TLS algorithms (Vicari, Zheng) The reference LDP approach consistently produced results comparable to the TLS algorithms but had limitations due to securing access to upper parts of canopies and in accurately estimating LIAD where there was complex leaf curvature. Overall, the TLS-based methods were shown to have the potential to provide a more comprehensive representation of the canopy structure, capturing the entire height profile and overcoming the limitations of the LDP approach.

The scope of the current study was restricted to stand-alone, individual trees. In future studies, the dataset could be extended to natural, real (i.e. forest stand) situations, including dense and overlapping crowns, with a gradient of canopy density. This study may serve as a template for establishing benchmark datasets, evaluation protocols, and accessibility of algorithms that could facilitate systematic comparisons of LIAD estimation algorithms, similar to the RAdiation transfer Model Intercomparison (RAMI) exercise (Widlowski *et al.*, 2015). This collaborative effort promotes fairness, reproducibility, and the advancement of LIAD estimation techniques by enabling researchers to identify strengths, weaknesses, and areas for improvement in their algorithms.

Acknowledgements

CM and JP were supported by the Estonian Research Council Grant PRG 1405. JP was supported by the Estonian Ministry of Education and Research, Centre of Excellence for Sustainable Land Use (TK232). DS received funding from the European Research Council (ERC) under the European Union's Horizon 2020 research and innovation programme (grant agreement no. 771049). AS received funding from the BIOSPACE project funded by the European Research Council (ERC) under the European Union's Horizon 2020 research and innovation programme (grant agreement no. 834709). The article reflects only the authors' view, and the Agency is not responsible for any use that may be made of the information it contains. JL received funding from the National Natural Science Foundation of China (no. 42471418) and the Jiangsu Natural Science Foundation (no. BK20241884). AELS received funding from the NASA Biodiversity Program (NNH20ZDA001N-BIODIV). BNB was supported by the United States Department of Agriculture National Institute of Food and Agriculture, Hatch project no. 1013396, and U.S. National Science Foundation grant IOS 2047628. The authors would like to thank three anonymous reviewers for their comments that helped to improve the initial submission of this manuscript.

Competing interests

None declared.

Author contributions

CMM, JP and AS planned and designed the research. CMM performed the experiments. JP, DS and MBV conducted fieldwork. CMM, DS and BNB pre-processed the data. BNB, JL, AELS, MBV and GZ provided source codes for their algorithms. AS helped with the critical discussion. CMM wrote and JP compiled the submitted version of the manuscript with input from all authors. CMM and JP share joint first authorship of this work.

ORCID

Brian N. Bailey https://orcid.org/0000-0003-1919-2324
Jing Liu https://orcid.org/0000-0001-5207-7614
Jan Pisek https://orcid.org/0000-0003-0396-2072
Daniel Schraik https://orcid.org/0000-0002-7794-3918
Andrew Skidmore https://orcid.org/0000-0002-6344-9273
Atticus E. L. Stovall https://orcid.org/0000-0001-9512-3318
Matheus Boni Vicari https://orcid.org/0000-0001-8841-4205
Guang Zheng https://orcid.org/0000-0003-4118-7804

Data availability

The TLS algorithms used in this study can be found at the following repositories: https://github.com/PlantSimulationLab/Helios (Bailey); TLSLeAF: https://github.com/aestovall/TLSLeAF (TLSLeAF); https://github.com/mattbv/lidar_leaf_properties (Vicari); https://pointclouds.org/ (PCL – more information on retrieval of point normals with this approach: https://pointclouds.org/documentation/tutorials/normal_estimation.html); https://github.com/qingfengxitu/leaf_angle_TLSpc (Liu); https://doc.cgal.org/latest/Point_set_processing_3/index.html#Point_set_processing_3NormalEstimation (Zheng). The source data for this study are available via Figshare Digital Repository (10.6084/m9.figshare.28573253).

References

Asner GP. 1998. Biophysical and biochemical sources of variability in canopy reflectance. *Remote Sensing of Environment* **64**: 234–253.

Aspose.3D Product Family. n.d. [WWW document] URL https://docs.aspose.com/3d/ [accessed 11 April 2023].

Bailey BN. 2019. HELIOS: a scalable 3D plant and environmental biophysical modeling framework. *Frontiers in Plant Science* **10**: 470023.

Bailey BN, Mahaffee WF. 2017. Rapid, high-resolution measurement of leaf area and leaf orientation using terrestrial LiDAR scanning data. *Measurement Science and Technology* **28**: 64006.

Chianucci F, Pisek J, Raabe K, Marchino L, Ferrara C, Corona P. 2018. A dataset of leaf inclination angles for temperate and boreal broadleaf woody species. *Annals of Forest Science* **75**: 2.

Darwin C. 1881. Movements of plants. *Nature* **23**: 409.

De Wit CT. 1965. *Photosynthesis of leaf canopies (no. 663).* Wageningen, the Netherlands: Pudoc. [WWW document] URL https://library.wur.nl/WebQuery/wurpubs/413358.

Disney M. 2019. Terrestrial LiDAR: a three-dimensional revolution in how we look at trees. *New Phytologist* **222**: 1736–1741.

Ehleringer J, Forseth I. 1980. Solar tracking by plants. *Science* **210**: 1094–1098.

Foundation B. n.d. *Blender.org—home of the blender project—free and open 3D creation software. Blender.Org.* [WWW document] URL https://www.blender.org/ [accessed 28 April 2023].

Goel NS, Strebel DE. 1984. Simple beta distribution representation of leaf orientation in vegetation canopies 1. *Agronomy Journal* **76**: 800–802.

Grotti M, Calders K, Origo N, Puletti N, Alivernini A, Ferrara C, Chianucci F. 2020. An intensity, image-based method to estimate gap fraction, canopy openness and effective leaf area index from phase-shift terrestrial laser scanning. *Agricultural and Forest Meteorology* **280**: 107766.

Helios Documentation v1.2.58. n.d. [WWW document] URL https://baileylab.ucdavis.edu/software/helios/ [accessed 28 April 2023].

Hosoi F, Omasa K. 2006. Voxel-based 3-D modeling of individual trees for estimating leaf area density using high-resolution portable scanning lidar. *IEEE Transactions on Geoscience and Remote Sensing* **44**: 3610–3618.

Itakura K, Hosoi F. 2019. Estimation of leaf inclination angle in three-dimensional plant images obtained from lidar. *Remote Sensing* **11**: 344.

Jin S, Tamura M, Susaki J. 2016. A new approach to retrieve leaf normal distribution using terrestrial laser scanners. *Journal of Forestry Research* **27**: 631–638.

Kellner JR, Albert LP, Burley JT, Cushman KC. 2019. The case for remote sensing of individual plants. *American Journal of Botany* **106**: 1139–1142.

Kissling WD, Shi Y, Koma Z, Meijer C, Ku O, Nattino F, Seijmonsbergen AC, Grootes MW. 2022. Laserfarm – a high-throughput workflow for generating geospatial data products of ecosystem structure from airborne laser scanning point clouds. *Ecological Informatics* **72**: 101836.

Koma Z, Zlinszky A, Bekő L, Burai P, Seijmonsbergen AC, Kissling WD. 2021. Quantifying 3D vegetation structure in wetlands using differently measured airborne laser scanning data. *Ecological Indicators* **127**: 107752.

Konishi A, Eguchi A, Hosoi F, Omasa K. 2009. 3D monitoring spatio–temporal effects of herbicide on a whole plant using combined range and chlorophyll a fluorescence imaging. *Functional Plant Biology* **36**: 874–879.

Kuusk A. 2020. Leaf orientation measurement in a mixed hemiboreal broadleaf forest stand using terrestrial laser scanner. *Trees* **34**: 371–380.

Lemeur R, Blad BL. 1974. A critical review of light models for estimating the shortwave radiation regime of plant canopies. *Agricultural Meteorology* **14**: 255–286.

Li Y, Guo Q, Su Y. 2018a. Retrieving the leaf area index of individual trees and stands using single-scan data from a terrestrial laser scanner. In: *IGARSS 2018–2018 IEEE international geoscience and remote sensing symposium.* Valencia, Spain: IEEE, 7536–7539.

Li Y, Su Y, Hu T, Xu G, Guo Q. 2018b. Retrieving 2-D leaf angle distributions for deciduous trees from terrestrial laser scanner data. *IEEE Transactions on Geoscience and Remote Sensing* **56**: 4945–4955.

Liu J, Skidmore AK, Wang T, Zhu X, Premier J, Heurich M, Beudert B, Jones S. 2019. Variation of leaf angle distribution quantified by terrestrial LiDAR in natural European beech forest. *ISPRS Journal of Photogrammetry and Remote Sensing* **148**: 208–220.

McKnight PE, Najab J. 2010. Mann-Whitney U test. In: Guha M, ed. *The corsini encyclopedia of psychology.* Hoboken, NJ, USA: John Wiley & Sons, Ltd, 1.

McNeil BE, Fahey RT, King CJ, Erazo DA, Heimerl TZ, Elmore AJ. 2023. Tree crown economics. *Frontiers in Ecology and the Environment* **21**: 40–48.

McNeil BE, Pisek J, Lepisk H, Flamenco EA. 2016. Measuring leaf angle distribution in broadleaf canopies using UAVs. *Agricultural and Forest Meteorology* **218**: 204–208.

Moskal LM, Zheng G. 2012. Retrieving forest inventory variables with terrestrial laser scanning (TLS) in urban heterogeneous forest. *Remote Sensing* **4**: 1–20.

Muraoka H, Takenaka A, Tang Y, Koizumi H, Washitani I. 1998. Flexible leaf orientations of *Arisaema heterophyllum* maximize light capture in a forest understorey and avoid excess irradiance at a deforested site. *Annals of Botany* **82**: 297–307.

Myneni RB, Ross J, Asrar G. 1989. A review on the theory of photon transport in leaf canopies. *Agricultural and Forest Meteorology* **45**: 1–153.

Niinemets Ü. 2010. A review of light interception in plant stands from leaf to canopy in different plant functional types and in species with varying shade tolerance. *Ecological Research* **25**: 693–714.

Ollinger SV. 2011. Sources of variability in canopy reflectance and the convergent properties of plants. *New Phytologist* **189**: 375–394.

Omasa K, Hosoi F, Konishi A. 2007. 3D lidar imaging for detecting and understanding plant responses and canopy structure. *Journal of Experimental Botany* **58**: 881–898.

Pepe M, Ackermann S, Fregonese L, Achille C. 2016. 3D point cloud model color adjustment by combining terrestrial laser scanner and close range photogrammetry datasets. *International Journal of Computer and Information Engineering* **10**: 1942–1948.

Pfennigbauer M, Ullrich A. 2010. Improving quality of laser scanning data acquisition through calibrated amplitude and pulse deviation measurement. *Proceedings of Laser Radar Technology and Applications XV* **7684**: 463–472.

Pisek J, Ryu Y, Alikas K. 2011. Estimating leaf inclination and G-function from leveled digital camera photography in broadleaf canopies. *Trees* **25**: 919–924.

Pisek J, Sonnentag O, Richardson AD, Mõttus M. 2013. Is the spherical leaf inclination angle distribution a valid assumption for temperate and boreal broadleaf tree species? *Agricultural and Forest Meteorology* **169**: 186–194.

Point Cloud Library. n.d. Point cloud library. [WWW document] URL https://pointcloudlibrary.github.io/ [accessed 28 April 2023].

Raabe K, Pisek J, Sonnentag O, Annuk K. 2015. Variations of leaf inclination angle distribution with height over the growing season and light exposure for eight broadleaf tree species. *Agricultural and Forest Meteorology* **214**: 2–11.

Ross J. 1975. Radiative transfer in plant communities. In: Monteith JL, ed. *Vegetation and the atmosphere*, vol. 1. London, UK: Academic Press, 13–55.

Ross J. 1981. *The radiation regime and architecture of plant stands.* Dordrecht, the Netherlands: Springer Netherlands.

Ryu Y, Sonnentag O, Nilson T, Vargas R, Kobayashi H, Wenk R, Baldocchi DD. 2010. How to quantify tree leaf area index in an open savanna ecosystem: a multi-instrument and multi-model approach. *Agricultural and Forest Meteorology* **150**: 63–76.

Stovall AEL, Masters B, Fatoyinbo L, Yang X. 2021. TLSL e AF: automatic leaf angle estimates from single-scan terrestrial laser scanning. *New Phytologist* **232**: 1876–1892.

Stuckens J, Somers B, Delalieux S, Verstraeten WW, Coppin P. 2009. The impact of common assumptions on canopy radiative transfer simulations: A case study in Citrus orchards. *Journal of Quantitative Spectroscopy and Radiative Transfer* **110**: 1–21.

Tadrist L, Saudreau M, de Langre E. 2014. Wind and gravity mechanical effects on leaf inclination angles. *Journal of Theoretical Biology* **341**: 9–16.

The Computational Geometry Algorithms Library. n.d. [WWW document] URL https://www.cgal.org/index.html [accessed 28 April 2023].

Utsugi H, Araki M, Kawasaki T, Ishizuka M. 2006. Vertical distributions of leaf area and inclination angle, and their relationship in a 46-year-old *Chamaecyparis obtusa* stand. *Forest Ecology and Management* **225**: 104–112.

Vicari MB. 2017. tlseparation: performs the wood/leaf separation from 3D point clouds generated using terrestrial LiDAR scanners (1.3.3) [PYTHON]. [WWW document] URL https://github.com/TLSeparation/source [accessed 8 May 2023].

Vicari MB, Pisek J, Disney M. 2019. New estimates of leaf angle distribution from terrestrial LiDAR: comparison with measured and modelled estimates from nine broadleaf tree species. *Agricultural and Forest Meteorology* **264**: 322–333.

Wang WM, Li ZL, Su HB. 2007. Comparison of leaf angle distribution functions: effects on extinction coefficient and fraction of sunlit foliage. *Agricultural and Forest Meteorology* **143**: 106–122.

Weber J, Penn J. 1995. Creation and rendering of realistic trees. In: Mair SG, Cook R, eds. *Proceedings of the 22nd annual conference on computer graphics and interactive techniques*. New York, NY, USA: Association for Computing Machinery, 119–128.

Widlowski JL, Mio C, Disney M, Adams J, Andredakis I, Atzberger C, Brennan J, Busetto L, Chelle M, Ceccherini G *et al.* 2015. The fourth phase of the radiative transfer model intercomparison (RAMI) exercise: actual canopy scenarios and conformity testing. *Remote Sensing of Environment* **169**: 418–437.

Yang X, Li R, Jablonski A, Stovall AEL, Kim J, Yi K, Ma Y, Beverly D, Phillips R, Novick K *et al.* 2023. Leaf angle as a leaf and canopy trait: Rejuvenating its role in ecology with new technology. *Ecology Letters* **26**: 1005–1020.

Yang X, Strahler AH, Schaaf CB, Jupp DLB, Yao T, Zhao F, Wang Z, Culvenor DS, Newnham GJ, Lovell JL *et al.* 2013. Three-dimensional forest reconstruction and structural parameter retrievals using a terrestrial full-waveform lidar instrument (Echidna®). *Remote Sensing of Environment* **135**: 36–51.

Zhao K, García M, Liu S, Guo Q, Chen G, Zhang X, Zhou Y, Meng X. 2015. Terrestrial lidar remote sensing of forests: maximum likelihood estimates of canopy profile, leaf area index, and leaf angle distribution. *Agricultural and Forest Meteorology* **209**: 100–113.

Zheng G, Moskal LM. 2012. Leaf orientation retrieval from terrestrial laser scanning (TLS) data. *IEEE Transactions on Geoscience and Remote Sensing* **50**: 3970–3979.